ISSN 1027-4510, Journal of Surface Investigation: X-ray, Synchrotron and Neutron Techniques, 2023, Vol. 17, Suppl. 1, pp. S78–S89. © Pleiades Publishing, Ltd., 2023.

Designing a Universal Undulator Beamline for Materials Science: A Conceptual Approach

I. P. Dolbnya[a], I. A. Bataev[b], Ya. V. Rakshun[c, d, *], V. A. Chernov[c], Yu. V. Khomyakov[c, e], M. V. Gorbachev[b], N. I. Chkhalo[f], D. A. Krasnorutsky[b], V. S. Naumkin[b, g], A. N. Sklyarov[e], N. A. Mezentsev[c], and A. M. Korsunsky[h]

[a] *Diamond Light Source, Harwell Science and Innovation Campus, Didcot, Oxfordshire, OX11 0DE UK*

[b] *Novosibirsk State Technical University, Novosibirsk, 630073 Russia*

[c] *Budker Institute of Nuclear Physics, Siberian Branch, Russian Academy of Sciences, Novosibirsk, 630090 Russia*

[d] *Siberian State University of Telecommunications and Information Science, Novosibirsk, 630102 Russia*

[e] *Novosibirsk State University, Novosibirsk, 630090 Russia*

[f] *Institute for Physics of Microstructures, Russian Academy of Sciences, Nizhny Novgorod, 607680 Russia*

[g] *Kutateladze Institute of Thermophysics, Siberian Branch, Russian Academy of Sciences, Novosibirsk, 630090 Russia*

[h] *Department of Engineering Science, University of Oxford, Parks Road, Oxford, OX1 3PJ UK*

**e-mail: Ya.V.Rakshun@inp.nsk.su*

Received January 21, 2023; revised March 15, 2023; accepted March 15, 2023

Abstract—We present the conceptual design of a universal materials-research beamline based on the undulator of a fourth-generation synchrotron-radiation source. The distinctive feature of the beamline is its capability to work with both spectrally narrow ($\Delta E/E \sim 10^{-4}$) and relatively broad, high-intensity radiation beams (5×10^{-2}). The optical scheme enables rapid switching between diffraction, radiographic, and spectroscopic experimental methods while keeping the beam's position fixed on the test sample and varying the spot size of the radiation from 100 nm to 1 mm.

Keywords: synchrotron radiation, materials science, in situ, X-ray diffraction, Laue diffraction, X-ray imaging, XAFS, extended undulator harmonics, submicrometer focusing, double-mirror multilayer monochromator, quadruple-crystal monochromator, Kirkpatrick–Baez mirrors

DOI: 10.1134/S1027451023070091

INTRODUCTION

X-ray diffraction and radiography methods, including coherent diffraction imaging and ptychography, are among the most sought-after techniques in materials science. Therefore, we designed a beamline to implement these methods using both monochromatic and "pink" beams. It was created to facilitate research using techniques such as small-angle and ultra-small-angle X-ray scattering, anomalous scattering, diffraction anomalous fine structure (DAFS) spectroscopy, X-ray fluorescence analysis, X-ray absorption fine structure (XAFS) spectroscopy, and quick X-ray absorption fine structure (QXAFS) spectroscopy. The beamline can also implement X-ray diffraction tomography and X-ray microscopy, including phase-contrast methods.

The developed beamline can be reconfigured rapidly (on the order of seconds) between diffraction and radiographic methods. It is optimized to operate in three modes with characteristic spot sizes on the sample of 1 mm (nonfocused, collimated beam), 10 μm, and approximately 100 nm with focusing. It enables the same spot on the sample to be maintained during energy scanning (including in broad ranges) or reconfiguration of the main optics.

The following operating modes are suggested (final focus optics can be introduced into the beam as needed): for traditional diffraction methods, a transfocator, a double-mirror monochromator, and a four-crystal monochromator in various combinations can be utilized. The insertion device operates in the standard mode (energy range 10–30 keV); for Laue diffraction, it operates in the extended-harmonic generation mode (energy range 15–25 keV, tuning to the fifth and seventh harmonics separately), with the primary optical elements being the transfocator and/or the double-mirror monochromator. In XAFS studies, the insertion device also works in the extended-harmonic generation mode, with the main optical elements being the transfocator, double-mirror monochromator, and four-crystal monochromator. The use of the four-crystal monochromator also enables

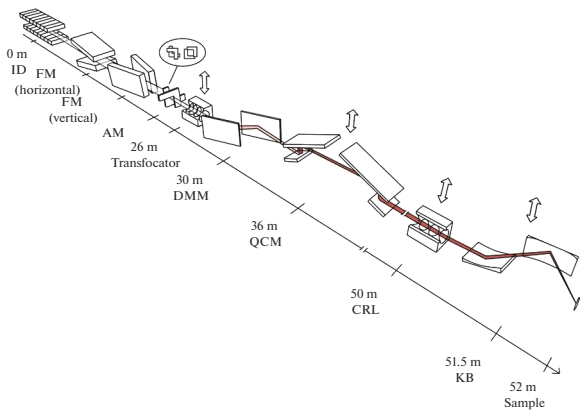

Fig. 1. Optical scheme of the beamline: ID is the insertion device; FM is the fixed mask; AM is the adjustable mask; Transfocator is a set of composite refractive lenses; DMM (double multilayer monochromator) is a two-mirror monochromator; QCM (quadruple crystal monochromator) is a four-crystal monochromator; CRL is a set of composite refractive lenses of final focus; KB is Kirkpatrick–Baez mirrors of the final focus.

QXAFS methods with data-acquisition frequencies up to 1 kHz; for microradiography methods (including 3D microtomography and ptychography), the transfocator and the double-mirror monochromator can be employed. We assume that the primary operating mode of the insertion device is standard, but operations in the extended-harmonic generation mode can also be performed. To address tasks using small-angle and ultra-small-angle X-ray scattering, a combination of optical components, including a transfocator, a double-mirror monochromator, and a four-crystal monochromator, is used in different configurations (the insertion device operates in its regular mode). X-ray fluorescence analysis is regarded as an auxiliary research technique, and its implementation can be easily carried out in conjunction with other methods by installing a semiconductor detector.

BEAMLINE DESIGN

The optical scheme of the beamline is shown in Fig. 1. To obtain radiation spots of various sizes on the sample (ranging from 100 nm to 1 mm), the following optical components are used: a transfocator (a set of beryllium refractive lenses), compound refractive lenses, and Kirkpatrick–Baez (KB) mirrors.

The following operating modes of beamline focusing optics are assumed: optics removed from the beam (without focusing); collimation of the radiation by a transfocator; 1 : 1 focusing using a transfocator (working in converging beams is possible); 25 : 1 focusing using compound refractive lenses (no collimation); focusing using composite refractive lenses (with collimation by a transfocator); 100 : 1 focusing using KB mirrors (without collimation, composite refractive lenses removed from the beam); focusing using KB mirrors (with collimation by a zoom lens, composite refractive lenses removed from the beam).

In each of the listed modes, the primary monochromatization of radiation (1 or 5%) is carried out using a two-mirror monochromator. To obtain narrower spectral bands, a four-crystal monochromator is used, and a two-mirror monochromator ensures a significant decrease in the thermal load on the first crystal of the four-crystal monochromator.

In X-ray optical calculations, the following parameters of the SKIF source were used: electron energy of 3 GeV, operating current of 400 mA (under injection conditions at full energy (top up)), emittance of 76 pm rad, and the values of β_x and β_y at the center of the rectilinear gap are 0.53 and 3.04 m, respectively.

Insertion Device

A two-section short-period superconducting undulator has been considered as a synchrotron-radiation source (insertion device). It is assumed that the sections are connected with a three-pole phase corrector. The presence of two sections and the ability to adjust currents in the coil sets (segments [1]) allow for the generation of harmonics with spectral widths of 1% (standard mode) and 5% (extended harmonics, "pink" beams). Optimization of the insertion-device parameters was carried out for the energy range of 10–30 keV (primary range), with the condition of maximizing the radiation flux through the front-end aperture.

Calculations for the insertion device were carried out using the SPECTRA 11 program [2] based on the specified magnetic field of the undulator. The optimal device parameters are as follows: two sections (with both sections being identical), a magnetic-field period of 13.5 mm, 140 periods in each section, 10 segments (each segment containing 14 periods), a magnetic-field strength of 1.08 T, and a total radiation power from the insertion device of 10 kW. The maximum magnetic field corresponds to an undulator parameter of $K = 1.36$, with the energy of the first harmonic being 3.3 keV. A phase error of 3° was assumed.

Angular and spatial parameters of harmonics in the standard mode were as follows: divergence (root-mean-square value, RMS) was 14.3 × 0.2, 13.6 × 10.2, 13.2 × 10.2, and 12.6 × 10.5 μrad for harmonics nos. 3, 5, 7, and 9, respectively; the source size (full-width at half maximum, FWHM) was 18.3 × 15.4, 17.7 × 15.4, 17.3 × 15.8, and 16.7 × 16.0 μm for the same harmonics, respectively. The angular aperture of the primary slits corresponds to $6\sigma_{x'} \times 6\sigma_{y'}$ of the first operating harmonic of the undulator (the third harmonic); it is 86 × 61 μrad.

In the mode of extended (5%) harmonics, the beam profiles in the center of the insertion device are calculated in the wiggler approximation and are (FWHM) 17.5 × 24.2 and 17.5 × 22.5 μm for the fifth

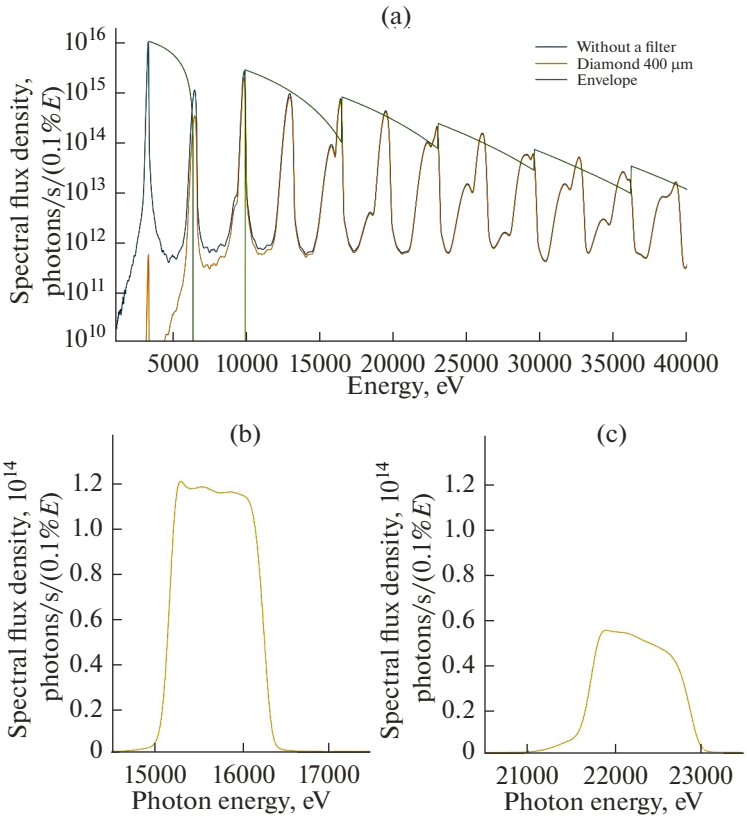

Fig. 2. Spectral flux density (in the range of a width of 0.1% of the energy E) through an aperture of (a) 86 × 61 μrad and its envelope when varying the coil currents (without filters) in the standard mode of the insertion device, and 45 × 45 μrad (with a diamond filter) in the modes (5%) of (b) the fifth and (c) seventh extended harmonics.

and seventh harmonics, respectively. We selected an angular aperture of 45 × 45 μrad to transmit a relatively uniform central part of the extended harmonic.

The spectral radiation density is shown in Fig. 2. By varying the currents in the coils of the insertion device, we can select an energy suitable for experiments in the range of 10–30 keV (envelope in Fig. 2a). To suppress unused fundamental harmonics and decrease the thermal load on the optics, we planned to install a 400-μm-thick diamond filter in the front end. The spectral density in the standard mode when using a diamond filter is shown in Fig. 2a. The radiation power emerging from the front end in the 86 × 61 μrad aperture is 286 W; the diamond filter absorbs 239 W. The radiation power in the 45 × 45 μrad aperture in the extended fifth and seventh harmonic modes is approximately 124 W; the diamond filter absorbs about 86 W. In further thermal calculations of the beamline optics, the standard operating mode of the insertion device was considered the one with the highest load.

Transfocator

The transfocator is located in an optical hutch immediately after the radiation-shielding wall (the first interface is situated 26 m from the radiation point) and is used for collimating or focusing the radiation in a 1 : 1 ratio. We selected the optimal radius of curvature (R) for lenses based on the criteria of maximizing the radiation flux while minimizing the number of sets of lenses needed to operate at different undulator harmonics. The radius of curvature, which ensures the lenses' geometric aperture is sufficient for transmitting each of the working harmonics, is R = 500 μm. In the calculations, standard beryllium lenses were used [3].

The parameters of the radiation, collimated or focused to a 1 : 1 ratio by the transfocator at a distance of 52 m from the radiation source, are presented in Table 1. Calculations were performed using the Shadow 3 program [4]. They accounted for double reflection from the multilayer mirrors of the double-mirror monochromator and absorption by additional filters. The Si/Be and Cr/Be multilayer mirrors are intended for the monochromatization of radiation in the standard undulator operating mode, and the mirrors with a W/Be coating are used for the undulator with extended harmonics (indicated by "e" in Table 1). The W/Be mirrors can also be used in the standard undulator operating mode. Figure 3 shows examples of images obtained from the source at a distance of 52 m.

Table 1. Beam parameters for collimation and 1 : 1 focusing modes (hereinafter, H and V are the horizontal and vertical spot sizes, respectively; FWHM is the full-width at half maximum)

Radiation parameters in the collimation mode							
photon energy, keV (harmonic no.)	number of lenses	focal length, m	size of the radiation spot on the sample, FWHM, μm		photon flux, photons/s		
			H	V	1%, Si/Be	1%, Cr/Be	4.6%, W/Be
9.9 (3)	3	24.0	690	490	7.09×10^{15}	–	–
16.4 (5)	8	24.7	660	510	3.40×10^{15}	2.57×10^{15}	2.36×10^{15}
23 (7)	14	25.9	710	580	–	8.57×10^{14}	6.29×10^{14}
29.6 (9)	25	25.7	600	520	–	2.46×10^{14}	–
16.4 (5e)	7	24.0	1086	1086	–	–	1.18×10^{15}
23 (7e)	14	25.3	1112	1113	–	–	2.13×10^{14}
Radiation parameters in the 1 : 1 focusing mode							
photon energy, keV (harmonic no.)	number of lenses	distance to the neck, m	size of the radiation spot on the sample, FWHM, μm		photon flux, photons/s		
			H	V	1%, Si/Be	1%, Cr/Be	4.6%, W/Be
9.9 (3)	5	29.9	27	21	6.57×10^{15}	–	–
16.4 (5)	14	28.6	33	27	3.10×10^{15}	2.35×10^{15}	2.15×10^{15}
23 (7)	28	27.0	29	26	–	7.38×10^{14}	5.41×10^{14}
29.6 (9)	47	26.6	23	23	–	2.03×10^{14}	–
16.4 (5e)	13	28.9	35	45	–	–	1.04×10^{15}
23 (7e)	28	26.5	29	35	–	–	1.72×10^{14}

For comparison, an image of the source in the absence of a transfocator is also given.

Monochromatization of Radiation

We plan to install two monochromators in the beamline: a horizontally reflecting double-mirror monochromator and a vertically reflecting four-crystal monochromator. It is assumed that the double-mirror monochromator is present in the beam in all beamline operating modes. It consists of a pair of flat multilayer mirrors and is designed for monochromatization of the synchrotron-radiation beam with $\Delta E/E$ of about 1 and 5% or, when used in conjunction with a four-crystal monochromator, for primary monochromatization and removal of the heat load from the first crystal of the four-crystal monochromator. This monochromator consists of a mirror-symmetric pair of Si(111) channel-cut monochromators and is intended for final monochromatization of the radiation ($\Delta E/E \sim 10^{-4}$). The main advantage of using a four-crystal monochromator is preservation of the

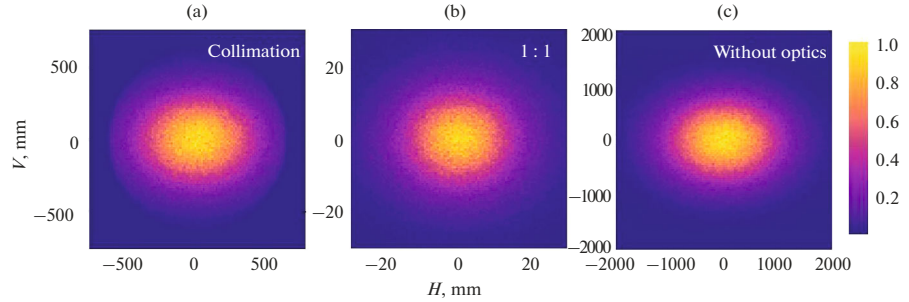

Fig. 3. Image of a source at a distance of 52 m, calculated for the third harmonic with (a) collimation, (b) 1 : 1 focusing, and (c) without optics; the flux density is given in arbitrary units.

Table 2. Parameters of multilayer coatings of a two-mirror monochromator (N is the number of layers, γ is the ratio of the thickness of the even sublayer to the thickness of the structure period)

No.	Coating	Period, Å	N	γ	Operating energy range, keV	$\Delta E/E$, %	Grazing angle, deg
1	Si/Be	76.6	300	0.33	9–16	1	0.3–0.5
2	Cr/Be	30	300	0.33	16–30	1	0.4–0.75
3	W/Be	38	150	0.40	16–25	4.6	0.4–0.6

position of the X-ray beam on the sample when implementing various research techniques at a single energy upon changing the radiation energy, introducing/withdrawing the four-crystal monochromator from the optical path, reconfiguring it for different undulator harmonics, or its operation with extended undulator harmonics in an experiment. An additional advantage of using a four-crystal monochromator is the ability to perform rapid energy scanning (QXAFS) with XANES-spectrum acquisition rates of up to 1 Hz.

The coating of the mirrors of the two-mirror monochromator consists of three strips 5 mm wide: Si/Be, Cr/Be, and W/Be. The Si/Be and Cr/Be pairs with $\Delta E/E = 1\%$ cover the main energy range of 10–30 keV, and the W/Be pair with $\Delta E/E = 4.6\%$ is designed to operate in the fifth and seventh extended harmonic modes (15–25 keV). The characteristics of the coatings are summarized in Table 2. Calculations were carried out taking into account a substrate roughness (RMS) of 3 Å and an interlayer roughness (RMS) of 3 Å using code [5] and XOP [6]. The grazing-angle range is from 0.3° (the fifth harmonic of the undulator, Si/Be mirrors) to 0.75° (the fifth harmonic of the undulator, Cr/Be mirrors). The optimal mirror length is around 300 mm. A schematic diagram of the monochromator is presented in [7].

Heat absorption by the mirrors is one of the most critical considerations when designing such a monochromator [8]. In the calculations, the operating mode with the highest load of the double-mirror monochromator was considered, with the highest grazing angle of 0.75° for the fifth harmonic of the undulator and Cr/Be mirrors (Fig. 4a), assuming complete radiation absorption. Thermal simulations of the mirror were conducted using the ANSYS 2020R2 software (Fluent module), using the steady-state temperature-field approximation with a surface heat distribution on the mirror's working lamella. The multilayer coating was not taken into account. The model specified conditions for radiative heat exchange with the surrounding environment for the lateral and lower surfaces of the mirror. Copper cooling radiators were placed on the lateral surfaces of the mirror. Following the methodology used in [8, 9], the radiators themselves were not included in the model; a heat transfer coefficient of 3000 W/(m^2 K) and a temperature of 295 K were set. The simulations considered the temperature-dependent thermophysical properties of silicon [10–13]. Deformation calculations (Fig. 4b) were performed using the ANSYS 2020R2 software (Static Structural module) while accounting for the data regarding the stationary volumetric temperature distribution. The main conclusion is the feasibility of using water-cooling for the double-mirror monochromator.

The first lamella of the four-crystal monochromator experiences the highest thermal load when transmitting the third harmonic (strip of the double-mirror monochromator from Si/Be), with a total radiation power of approximately 14 W. The corresponding Bragg angle for the maximum of the third harmonic is 11.63°. The power density in this case is illustrated in Fig. 4c.

To simplify thermal analysis, the temperature calculations and deformation simulations of the first crystal of the four-crystal monochromator were conducted using models constructed for the double-mirror monochromator. The results obtained (Fig. 4d) indicate that in the case of cryogenic cooling, the largest displacements are observed at the periphery of the beam and amount to approximately 0.3–0.4 μrad. This level of displacement is acceptable since it is significantly smaller than the linewidth of the Si(111) rocking curve at the corresponding energy.

The emission spectra after two reflections from the mirrors of the double-mirror monochromator in the standard mode, as well as the fifth and seventh extended harmonics, are presented in Fig. 5. To suppress the soft component of the total external reflection (TER) in the beamline, we proposed to install a set of foils made of various materials. The filter materials and their thicknesses are given in the figures. To assess the spectral purity, we used the harmonic coefficient Ch_n, defined as follows: $Ch_n = \sqrt{\sum_{i \neq n} F_i^2} / F_n \times 100\%$, where i is the number of the undulator harmonic, n is the number of the working harmonic, and F is the corresponding values of the spectral density of the photon flux. An example of the spectral photon-flux density (the fifth harmonic) after monochromatization by a two-mirror + four-crystal monochromator system in the normal mode and the extended-harmonic mode is shown in Fig. 5f.

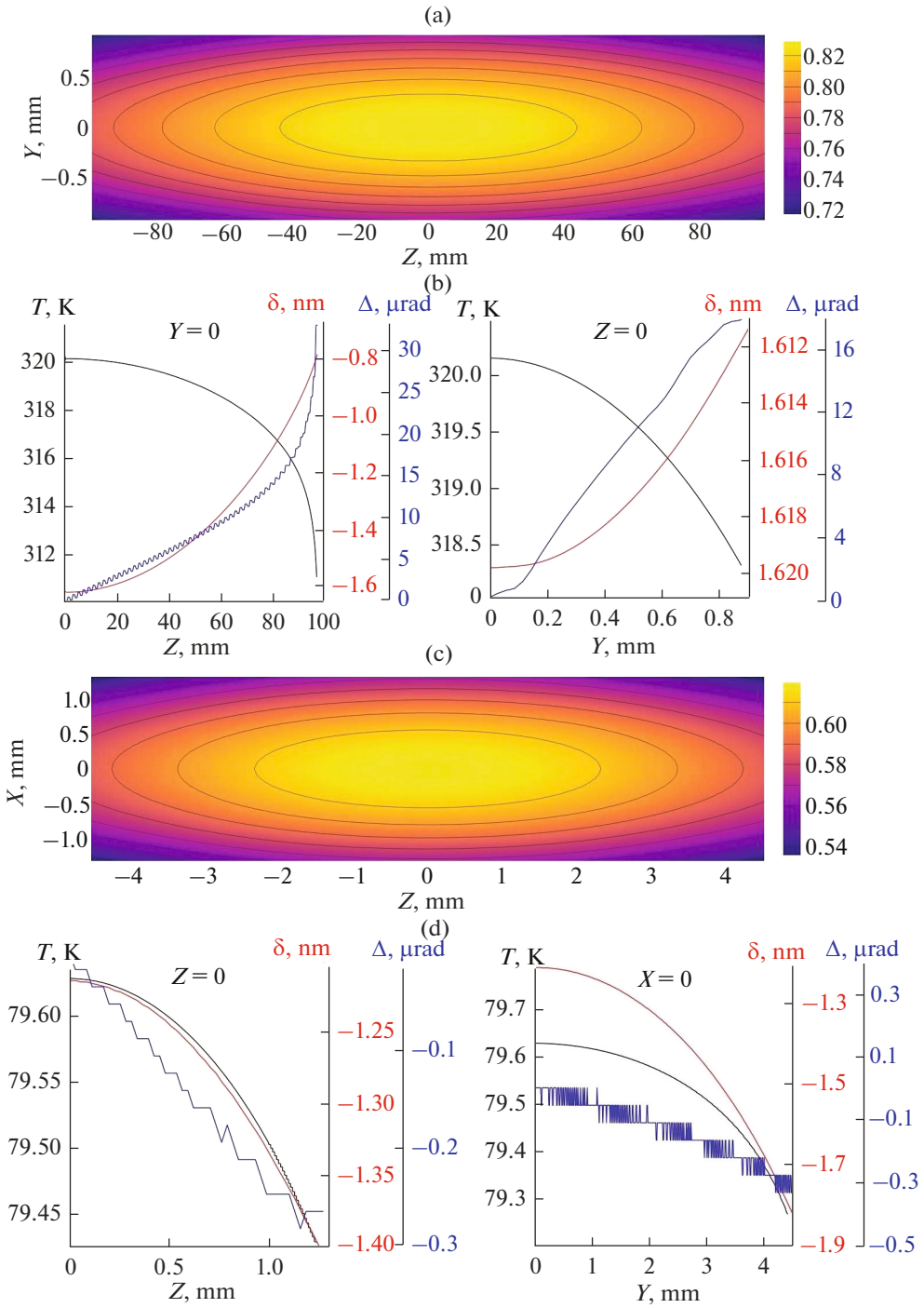

Fig. 4. Thermal calculations: (a) power density (W/mm^2) of radiation incident on the first multilayer mirror at a grazing angle of 0.75°; (b) temperature and displacement profiles in the middle sections for the first mirror; (c) power density (W/mm^2) of radiation incident on the first lamella of the four-crystal monochromator at a Bragg angle of 11.63°; (d) temperature and displacement profiles in the middle sections for the first lamella.

Final-Focus Optics

The first refractive surface of the composite refractive lenses designed for 25 : 1 focusing is located at a distance of 50 m from the center of the insertion device. The results of calculations of the final-focus lenses (made of beryllium) are presented in Table 3. The lens parabola radius $R = 200$ μm was selected so that its geometric aperture completely transmitted the beam collimated by the transfocator.

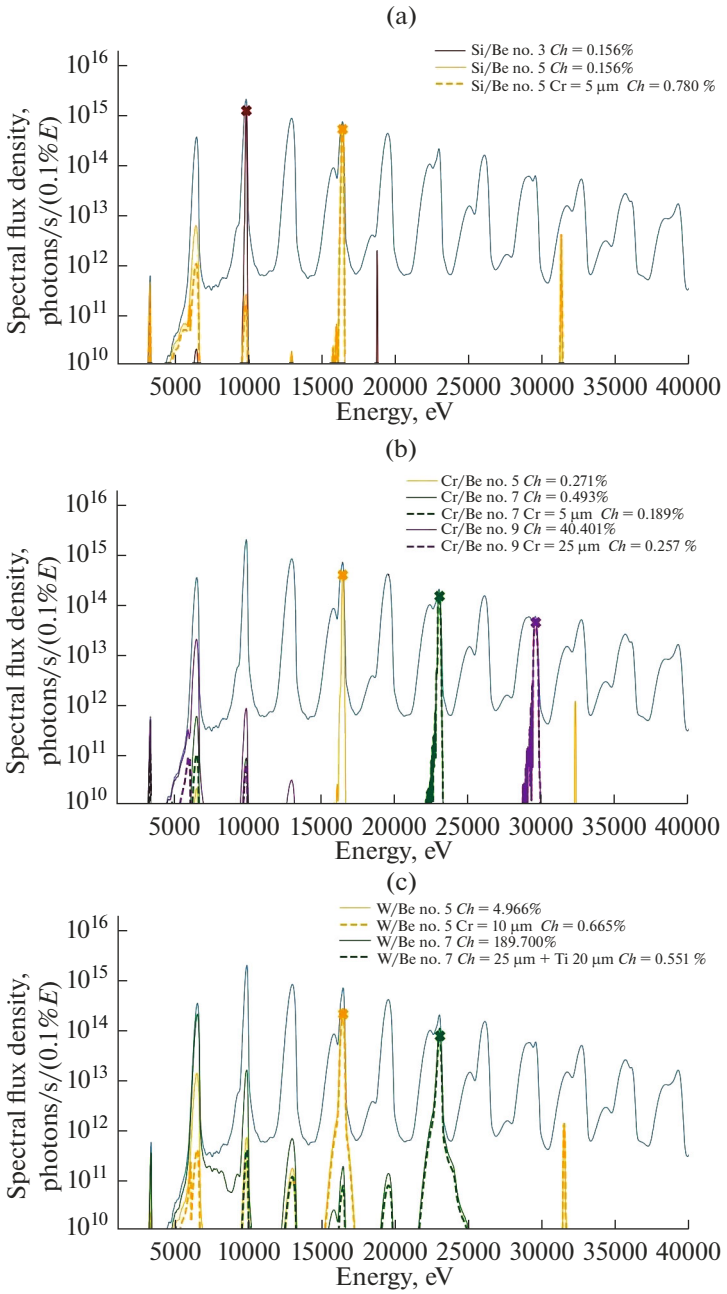

Fig. 5. Spectral photon flux density (in a range of a width of 0.1% of the energy E) after the two-mirror monochromator (a–c) in the standard operating mode of the insertion device and (d, e) in the mode of the fifth and seventh extended harmonics. Spectral photon flux density after the two-mirror and four-crystal monochromator (f) in the standard operating mode of the insertion device and (g) in the fifth extended-harmonic mode. *Ch* is the harmonic coefficient. The filter materials and their thickness are given.

To enhance the beamline radiation flux on the sample, we considered a scheme in which the compound refractive lenses of the final focus are used together with the transfocator in the collimation mode. The calculation results are presented in Table 4. In this case, the spot size on the sample increases to 2.5 μm, approximately 1.6 times larger, and the radiation flux increases threefold.

The Kirkpatrick–Baez (KB) mirrors consist of a pair of orthogonal mirrors with an elliptical profile. In the proposed scheme, the first mirror focuses the beam vertically, and the second one focuses it horizontally. To enable use across the entire working energy range and to have the ability to focus the radiation from extended harmonics, the use of TER mirrors was also suggested.

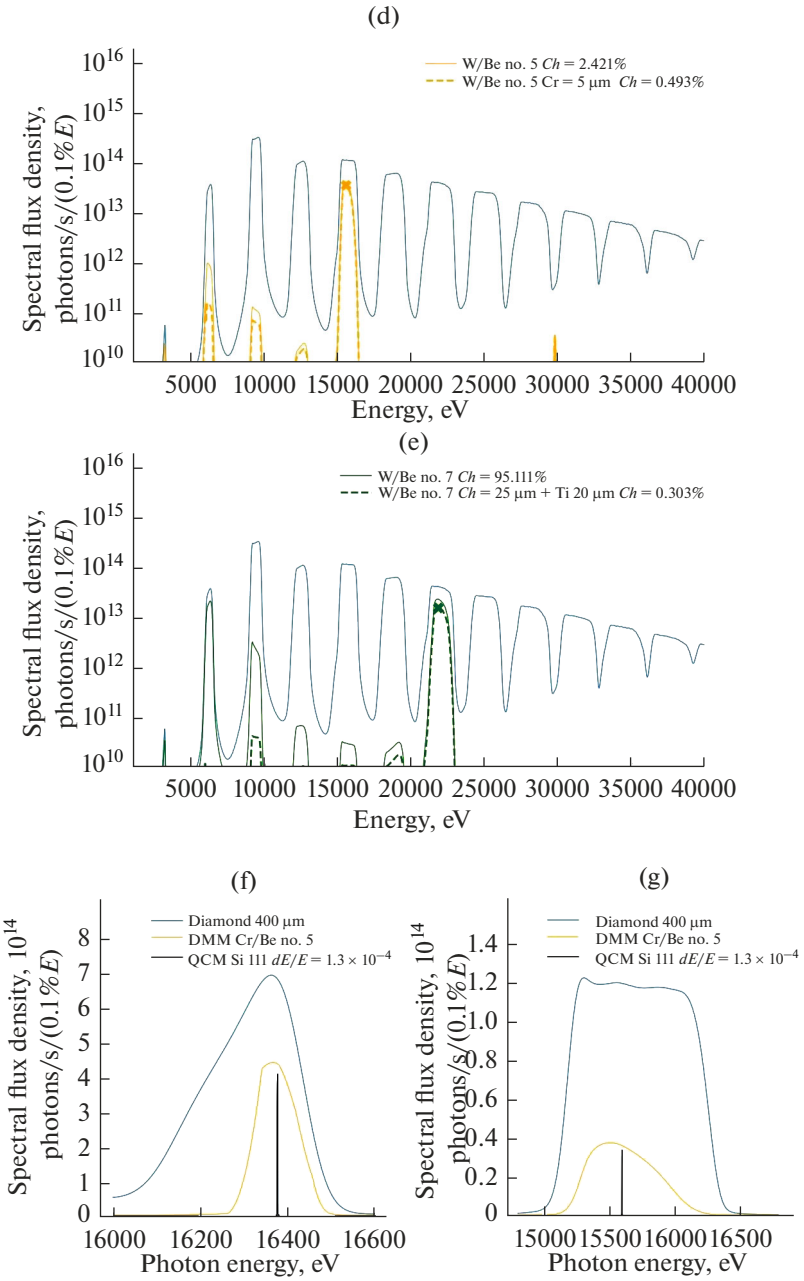

Fig. 5. (Contd.)

We considered iridium as a coating for the KB mirrors. The grazing angle for the energy range up to 30 keV, at which no less than 50% of the radiation is reflected during double reflection, is 2.75 mrad. The calculations were carried out, taking into account a surface roughness (RMS) of 3 Å, using the XOP code.

We optimized the mirrors based on the following conditions: the distance from the end of the second mirror to the focal plane (sample) should be at least 200 mm; the typical spot size on the sample is around 100 nm; the KB mirror system should capture the entire SR beam collimated by the transfocator. The 200-mm distance (with a free distance of 150–170 mm) was selected to ensure the placement of substantial power equipment for the sample environment. With mirror lengths of 300 mm, the geometric aperture of the system is approximately 825 × 825 μm. In this geometry, the center of the first mirror should be located at a distance of 51.34 m from the center of the insertion device, and the center of the second mirror, at a distance of 51.65 m. In this mode, the composite refractive lenses are removed from the optical path. The results of KB mirror calculations, using the Shadow code, are presented in Table 5. In the calcula-

Table 3. Beam parameters upon focusing with final-focus lenses

Photon energy, keV (harmonic no.)	Number of lenses	Distance to the neck, m	Size of the radiation spot on the sample, FWHM, μm		Photon flux, photons/s		
			H	*V*	1%, Si/Be	1%, Cr/Be	4.6%, W/Be
9.9 (3)	14	2090	1.64	1.4	9.76×10^{14}	–	–
16.4 (5)	40	2038	1.74	1.62	4.39×10^{14}	3.32×10^{14}	3.05×10^{14}
23 (7)	81	2011	1.48	1.66	–	8.54×10^{13}	6.26×10^{13}
29.6 (9)	138	2044	1.31	1.27	–	1.69×10^{13}	–
16.4 (5e)	35	2170	1.84	2.24	–	–	7.73×10^{13}
23 (7e)	72	2229	2.08	2.48	–	–	1.11×10^{13}

Table 4. Beam parameters in the "transfocator + final-focus lenses" focusing mode

Photon energy, keV (harmonic no.)	Size of the radiation spot on the sample, FWHM, μm		Photon flux, photons/s		
	H	*V*	1%, Si/Be	1%, Cr/Be	4.6%, W/Be
9.9 (3)	2.65	2.1	3.16×10^{15}	–	–
16.4 (5)	2.89	2.6	1.38×10^{15}	1.04×10^{15}	9.56×10^{14}
23 (7)	2.38	2.14	–	2.38×10^{14}	1.74×10^{14}
29.6 (9)	2.06	2.06	–	5.62×10^{13}	–
16.4 (5e)	2.88	3.92	–	–	2.83×10^{14}
23 (7e)	2.88	3.52	–	–	3.76×10^{13}

tions, a generated Shadow profile with a figure error of 1 nm (root-mean-square deviation from the ideal profile) was used. The slope error is approximately 70 nrad. The power of the radiation focused by the system can reach 3.2 W, and the power density at the center of the spot is 79 μW/nm^2.

To increase the radiation flux on the sample, a scheme was considered in which KB mirrors are used together with the transfocator in the collimation mode. In this case, the size of the radiation spot on the sample increases to 1.2 μm. The examples of images obtained using final-focus optics at a distance of 52 m from the source are shown in Fig. 6.

The above calculations are carried out in a geometric approximation. The transverse coherence length for radiation with the wavelength λ at a distance R from the source with RMS $\sigma_{x,y}$ is determined as [14]

$$t_c^{(t)}[\text{m}] = 28.21\frac{\lambda[\text{Å}]R[\text{m}]}{\sigma_{x,y}[\text{m}]}$$

for the third harmonic at a distance of 52 m from the source, $t_c^{(t)} \cong 260$ μm, which is significantly smaller than the apertures of KB mirrors (825 μm) and composite refractive lenses of the final focus (880 μm). At 1 : 1 focusing or collimation of the radiation with the transfocator, the transverse coherence length at a distance of 26 m from the source is half as large, 130 μm. For higher harmonics, $t_c^{(t)}$ is automatically smaller than all the mentioned apertures.

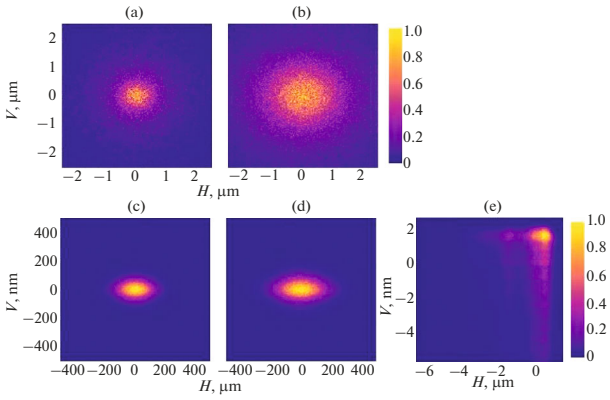

Fig. 6. Image of the source for the third harmonic of the undulator at a distance of 52 m when focusing: with (a) a set of composite refractive lenses of the final focus, (b) a transfocator and refractive lenses; (c) ideal KB mirrors, (d) KB mirrors with a standard deviation of 1 nm from the ideal mirror profile, and (e) a transfocator and KB mirrors with a standard deviation of 1 nm from the ideal mirror profile. The flux density is given in arbitrary units.

Table 5. Beam parameters in the focusing mode with KB mirrors (including together with the transfocator)

photon energy, keV (harmonic no.)	size of the radiation spot on the sample, FWHM, nm		photon flux, photons/s		
	H	*V*	1%, Si/Be	1%, Cr/Be	4.6%, W/Be
KB mirror					
9.9 (3)	248	109	1.99×10^{15}	–	–
16.4 (5)	248	109	7.97×10^{14}	6.03×10^{14}	5.54×10^{14}
23 (7)	257	109	–	2.09×10^{14}	1.53×10^{14}
29.6 (9)	257	129	–	3.82×10^{13}	–
16.4 (5e)	337	109	–	–	1.41×10^{14}
23 (7e)	317	109	–	–	2.68×10^{13}
Transfocator + KB mirror					
9.9 (3)	1270	1270	5.39×10^{15}	–	–
16.4 (5)	1270	1140	2.07×10^{15}	1.57×10^{15}	1.44×10^{15}
23 (7)	1110	980	–	4.80×10^{14}	3.52×10^{14}
29.6 (9)	1190	1230	–	9.75×10^{13}	–
16.4 (5e)	1180	1290	–	–	5.22×10^{14}
23 (7e)	1270	1270	–	–	8.97×10^{13}

"Sample Environment" System

A schematic diagram of the "environment" of the sample is shown in Fig. 7. Samples can be placed at two points: at a distance of 42–49 and 52 m from the radiation source. At distances of 42–49 m, the radiation beam is formed using the transfocator, two-mirror monochromator, and four-crystal monochromator in various combinations: radiation with "natural" divergence (the transfocator is removed from the beam); radiation collimated by the transfocator; converging beams (the transfocator at a distance of 26 m from the emission point in the 1 : 1 focusing mode).

At a distance of 52 m, the radiation beam is shaped using final-focus optics, including composite refractive lenses and KB mirrors. Various beam configurations are formed in addition to the transfocator, double-mirror monochromator, and four-crystal monochromator: radiation with "natural" divergence

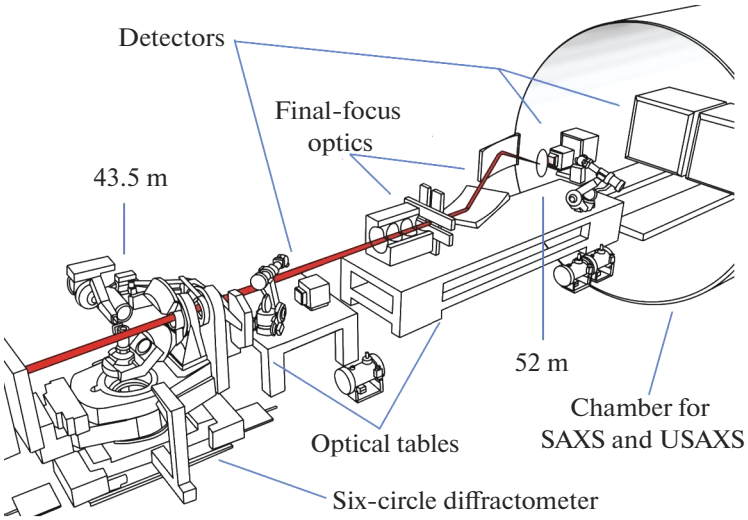

Fig. 7. Schematic diagram of the sample environment system. SAXS and USAXS are small-angle and ultra-small-angle X-ray scattering, respectively.

(transfocator removed from the beam); radiation collimated by the transfocator; beams focused 1 : 1 by the transfocator; beams focused 25 : 1 by composite refractive lenses; beams collimated by the transfocator and then focused by composite refractive lenses; beams focused 100 : 1 (possibly 150 : 1) by KB mirrors; and beams collimated by the transfocator and then focused by KB mirrors.

In both cases, monochromatization can be performed using a two-mirror monochromator with $\Delta E/E = 10^{-2}$ (operating range of 10–30 keV) or $\Delta E/E = 4.6 \times 10^{-2}$ (operating range 15–25 keV) or using two-mirror and four-crystal monochromators with $\Delta E/E = 1.3 \times 10^{-4}$ (operating range 10–30 keV).

At a distance of 42–45 m from the radiation source, we plan to install a diffractometer based on a multifunctional six-circle kappa goniometer for crystallographic research and a six-axis robot manipulator for automatic sample handling. At a distance of 45–47 m, a two-meter optical table will be positioned for the movement systems, sample manipulation, and detectors. In millimeter-sized beams, various techniques can be implemented, including monochromatic and "pink" beam diffraction, grazing incidence and transmission geometry diffraction, energy-dispersive diffractometry, and various types of X-ray imaging, including coherent imaging, X-ray fluorescence analysis, and XAFS spectroscopy. Additionally, there will be approximately 2 m of free space (47–49 m) for convenient logistics within the experimental hutch.

At a distance of 52 m from the radiation source, the station operates as a "materials-science microscope," providing a set of monochromatic and "pink" beams with characteristic sizes ranging from 100 nm to 1 mm, all converging to a single point. The final-focus optics, slits, sample, and detectors for wide-angle X-ray scattering, radiography, X-ray fluorescence, and XAFS spectroscopy, as well as a robotic arm for quick detector changes, are located on one long, 4-m optical table. Specialized devices for sample manipulation are also planned to be positioned on this table.

Behind the optical table, there is a vacuum chamber with a diameter of approximately 2 m and a length of up to 25 m, following a design similar to that proposed in [15]. Inside this chamber, two detectors mounted on independent rails are installed, each covering half of the space behind the sample. This setup is designed to facilitate the same research methods as mentioned before but in the "materials-science microscope" mode, as well as the small-angle and ultra-small-angle X-ray scattering methods. The combination of wide-angle and small-angle methods, including the adjustment of detector positions within the chamber, thus can be achieved.

CONCLUSIONS

The possibility of investigating materials at various structural levels (from surfaces, interfaces, grains, and their agglomerates to entire samples) is crucial in materials science. During submicroscopic in situ studies, where the beam size is on the order of hundreds of nanometers, the experimenter needs to have full confidence that the region under examination, where the beam is focused, remains consistent. The presented design concept of the materials-science beamline fulfills the following conditions: it offers a versatile optical solution for various experimental methods, high fluxes, and small beam sizes for in situ and operando research, and it operates as a "materials-science microscope," preserving the focal point. In other words, it serves as a conveyor for materials science.

ACKNOWLEDGMENTS

We are grateful to A. Trebushinin for his help in working on the insertion device for the beamline and A. Murzina for her help in preparing the figures.

FUNDING

This work was supported by ongoing institutional funding. No additional grants to carry out or direct this particular research were obtained.

CONFLICT OF INTEREST

The authors of this work declare that they have no conflicts of interest.

REFERENCES

1. A. Trebushinin, S. Serkez, M. Veremchuk, et al., J. Synchrotron Radiat. **28**, 769 (2021). https://doi.org/10.1107/S1600577521001958
2. T. Tanaka, J. Synchrotron Radiat. **28**, 1267 (2021). https://doi.org/10.1107/S1600577521004100
3. https://www.rxoptics.de/products/lenses/.
4. M. Sanchez del Río, N. Canestrari, F. Jiang, and F. Cerrina, J. Synchrotron Radiat. **18**, 708 (2011). https://doi.org/10.1107/S0909049511026306
5. M. Svechnikov, J. Appl. Crystallogr. **53**, 244 (2020). https://doi.org/10.1107/S160057671901584X
6. M. Sánchez del Río and R. J. Dejus, Proc. SPIE **8141**, 814115 (2011). https://doi.org/10.1117/12.893911
7. N. I. Chkhalo, S. A. Garakhin, I. V. Malyshev, et al., Zh. Tekh. Fiz. **92**, 1261 (2022).
8. P. Brumund, J. Reyes-Herrera, C. Morawe, et al., J. Synchrotron Radiat. **28**, 1423 (2021). https://doi.org/10.1107/S160057752100758X

9. Y. Li, A. M. Khounsary, J. Maser, and S. Nair, Proc. SPIE **5193**, 1 (2004). https://doi.org/10.1117/12.524908

10. L. Zhang, W.-K. Lee, M. Wulff, and L. Eybert, J. Synchrotron Radiat. **10**, 313 (2003). https://doi.org/10.1107/S0909049503012135

11. Y. Touloukian, R. Powell, C. Ho, and P. Klemens, *Thermophysical Properties of Matter* (Plenum, New York, 1970), **Vol. 1**. http://poplab.stanford.edu/pdfs/Touloukian-v1ThermalConductivityMetallicElementsAlloys-tprc70.pdf.

12. T. Middelmann, A. Walkov, G. Bartl, and R. Schödel, Phys. Rev. B **92**, 174113 (2015). https://doi.org/10.1103/PhysRevB.92.174113

13. H. Watanabe, N. Yamada, and M. Okaji, Int. J. Thermophys. **25**, 221 (2004). https://doi.org/10.1023/B:IJOT.0000022336.83719.43

14. P. Willmott, *An Introduction to Synchrotron Radiation. Techniques and Applications* (Willey, New York, 2019).

15. T. Narayanan, M. Sztucki, T. Zinn, et al., J. Appl. Crystallogr. **55**, 98 (2022). https://doi.org/10.1107/S1600576721012693

Translated by O. Zhukova